Title

Design of Surfactant Protein B Peptide Mimics Based on the Saposin Fold for Synthetic Lung Surfactants.

Journal

Biomedicine Hub, 1(3)

ISSN

2296-6870

Authors

Walther, Frans
Gordon, Larry
Waring, Alan

Publication Date

2016

DOI

10.1159/000451076

Peer reviewed

Biomedicine Hub

Biomed Hub 2016;1:451076 (DOI: 10.1159/000451076)

Received: August 4, 2016
Accepted after revision: September 27, 2016
Published online: November 16, 2016

Review

Design of Surfactant Protein B Peptide Mimics Based on the Saposin Fold for Synthetic Lung Surfactants

Frans J. Walther[a, b] Larry M. Gordon[a] Alan J. Waring[a, c]

[a]Los Angeles Biomedical Research Institute, Harbor-UCLA Medical Center, Torrance, CA, and Departments of [b]Pediatrics and [c]Medicine, David Geffen School of Medicine, University of California Los Angeles, Los Angeles, CA, USA

What Is It about?

Native lung surfactant plays a pivotal role in normal breathing because it reduces alveolar surface tension to low values. Its biophysical activity depends uniquely on the hydrophobic surfactant protein B (SP-B). Treatment with bovine and porcine lung surfactant extracts has greatly improved survival of premature infants with respiratory problems due to surfactant deficiency. SP-B is a member of the saposin family of proteins that share an overall three-dimensional folding pattern based on secondary structures and disulfide connectivity. Using the saposin 3D-structural motif, we designed, synthesized, and tested the surface activity of synthetic lung surfactants containing active SP-B mimics.

Keywords

Molecular design · Bioengineering · Mini-B · Super Mini-B · Saposin-like proteins · Synthetic lung surfactants · Phospholipase-resistant lipids · Neonatal respiratory distress syndrome · Acute lung injury/acute respiratory distress syndrome

Abstract

Surfactant protein (SP)-B is a 79-residue polypeptide crucial for the biophysical and physiological function of endogenous lung surfactant. SP-B is a member of the saposin or saposin-like proteins (SAPLIP) family of proteins that share an overall three-dimensional folding pattern based on secondary structures and disulfide connectivity and exhibit a wide diversity of biological functions. Here, we review the synthesis, molecular biophysics and activity of synthetic analogs of saposin proteins designed to mimic those interactions of the parent proteins with lipids that enhance interfacial activity. Saposin proteins generally interact with target lipids as either monomers or multimers via well-defined amphipathic helices, flexible hinge domains, and insertion sequences. Based on the known 3D-structural motif for the saposin family, we show how bioengineering techniques may be used to develop minimal peptide constructs that maintain desirable structural properties and activities in biomedical applica-

Frans J. Walther, MD, PhD, FAAP
Los Angeles Biomedical Research Institute
Harbor-UCLA Medical Center
1124 West Carson Street, Torrance, CA 90502 (USA)
E-Mail fjwalther@ucla.edu

tions. One important application is the molecular design, synthesis and activity of Saposin mimics based on the SP-B structure. Synthetic lung surfactants containing active SP-B analogs may be potentially useful in treating diseases of surfactant deficiency or dysfunction including the neonatal respiratory distress syndrome and acute lung injury/acute respiratory distress syndrome.

Introduction to Saposin Family Proteins

SP-B is a 79-residue polypeptide that is crucial for the biophysical and physiological function of endogenous pulmonary surfactant [1, 2]. SP-B is a member of the saposin or saposin-like proteins (SAPLIP) family of proteins based on amphipathic helical sequences, alignments, and disulfide connectivities [3, 4]. This combination of structural motifs results in a tertiary ensemble that incorporates amphipathic helices and turn/bend regions in a "saposin fold" structure stabilized by intramolecular disulfide linkages. This disposition of structural elements with stable helical regions plus specifically distributed charged residues and defined molecular flexibility promotes strong interactions with both the head groups and fatty chains of lipids [5, 6]. Over the past decade, structures have been determined for several saposin proteins (e.g., NK-lysin, saposins B and C) based on solution NMR and high-resolution X-ray crystallography [4–10]. These physical studies on saposins other than SP-B showed that the characteristic *saposin fold* consists of 4–5 α-helical domains (i.e., N-terminal helix 1, helices 2–4 and C-terminal helix 5) joined together by 2–3 intramolecular disulfide links [11]. The helical bundle for saposins is folded into two leaves, with one leaf having α-helices 1 and 4–5 and the second leaf composed of α-helices 2 and 3, with flexible hinges between helices 1 and 2 and also between helices 3 and 4–5. Saposins may fold in either *closed* or *opened* tertiary conformations. In the *closed* or compact conformation, the two leaves are in close contact such that the amphipathic α-helices with hydrophilic (charged, neutral) residues face the solvent, while hydrophobic side chains form a core stabilized by intramolecular disulfide bonds. In the *opened* or extended conformation, however, the two leaves of the saposin are splayed apart, thereby exposing more of the cationic and hydrophobic amino-acid residues for binding to lipids [11]. Although the complete three-dimensional (3D) structure of human SP-B has not yet been determined, homology modeling of SP-B, in which the primary sequence of SP-B was templated onto the known 3D structure of NK-lysin, indicated that SP-B may fold as a *closed* saposin [12–14]. Homology modeling is justified because the primary sequences and disulfide cross-linkages for both SP-B and many members of the Saposin family of proteins share a common evolutionary origin [3]. Here, the structure of human SP-B has been homology modeled based on the lowest energy conformers of NK-lysin, granulysin, saposin A, saposin C and saposin D [4, 6–9], which was then aligned with SP-B by sequence similarities using TM-align [15] followed by structural analysis using the server-based I-TASSER program [16]. This homology-modeled SP-B exhibits the typical folding pattern for closed saposins, with one leaf including the N-terminal insertion sequence and helix 1, C-terminal helix 5 and the leucine repeat helix 4 in close apposition, and the second leaf composed of the AV repeat helix 2 and Inner dimer helix 3 joined by the disulfide stabilized bend (Fig. 1). Although the complete 3D structure of full-length SP-B has not yet been experimentally determined, the N- and C-terminal helical domains have been confirmed with conventional and isotope-enhanced Fourier transform infrared (FTIR) [14, 17–19] and solution 2D-NMR [20–22] spectroscopic analyses of extensive peptide fragments based on the known primary sequence and/or disulfide connectivities of the parent SP-B.

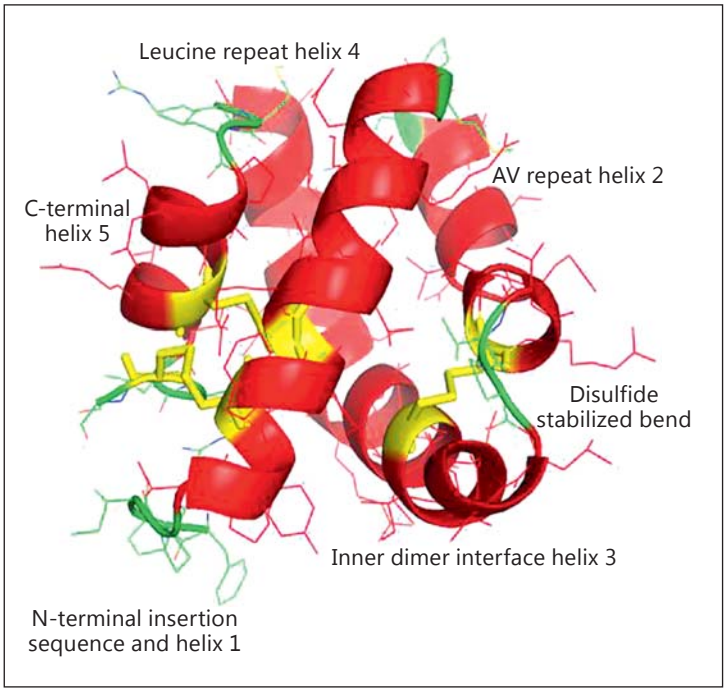

Fig. 1. A 3D homology model of SP-B that folds in the *closed* saposin conformation, constructed by templating the primary sequence of the target SP-B protein onto the lowest energy conformers of the experimental NK-lysin (PDB:1NKL), granulysin (PDB:1L9L), saposin-A (PDB:2DOB), saposin-C (PDB:2GTG), and saposin-D (PDB:3BQP) structures. Human SP-B and the saposin family proteins were aligned by sequence similarities using TM-align [15], followed by structural homology templating and refinement using the server-based I-TASSER program [16] (see Introduction to Saposin Family Proteins). This homology-modeled SP-B shows five amphipathic helices organized in two "leafs." The first leaf includes the N-terminal insertion sequence and helix 1, C-terminal helix 5, and the leucine repeat helix 4 in close apposition, while the second leaf is composed of the AV repeat helix 2 and inner dimer helix 3 joined by the disulfide stabilized bend. This homology model was used to design novel linear peptides (i.e., Mini-B and Super Mini-B) that when oxidized (i.e., disulfide-linked) not only closely simulate the 3D-structure of the leaf containing the N- and C-terminal helices, but also demonstrate high surfactant activities. Alpha helixes are highlighted in red, disulfide linkages are in yellow, bends and disordered backbone conformations are colored in green.

One important aspect of homology-based models of SP-B (e.g., Fig. 1) is that they predict disk-like structures containing disulfide-linked, positively charged amphipathic helices (i.e., N- and C-terminal domains), which may promote surfactant activity [12–14, 23]. In our laboratories [14, 19, 24], we have developed synthetic, disulfide cross-linked peptide constructs (e.g., the 34-residue "Mini-B" or "MB" and the 41-residue "Super Mini-B" or "S-MB"), which not only mimic the structure of the SP-B leaf containing the N- and C-terminal regions, but also demonstrate high surfactant activities in in vitro and in vivo assays. Because the importance of SP-B in respiratory function is directly linked to its activity in pulmonary surfactant, a discussion of this complex and essential biological material is given below and the therapeutic importance of synthetic lung surfactants is described. Subsequent sections then describe how this basic information was used to develop "short-cut" versions of full-length SP-B (e.g., MB and S-MB) that exhibit high surfactant activities.

Endogenous Lung Surfactant

Surfactant in the lungs of air-breathing animals is one of the most powerful surface-active substances known. Biophysically important chemical components of endogenous lung surfactant include dipalmitoyl phosphatidylcholine (DPPC), a mix of other saturated and unsaturated zwitterionic phosphatidylcholine (PC) species, anionic phospholipids including phosphatidylglycerol (PG), and three surfactant proteins (SPs): SP-A, SP-B, and SP-C. A fourth apoprotein (SP-D) is not involved in the biophysical functioning of lung surfactant. By lowering and varying alveolar surface tension, lung surfactant has physiologically essential actions in maintaining a low work of breathing and stabilizing small alveoli against collapse (atelectasis) during expiration. Lung surfactant also enhances the uniformity of alveolar inflation during inspiration, and reduces the overall hydrostatic driving force for pulmonary edema. Details of the discovery, composition, and physiological actions of pulmonary surfactant are reviewed elsewhere [1].

Lung Surfactant-Related Disease and Surfactant Therapies

Because active pulmonary surfactant is pivotal for normal breathing, its deficiency or dysfunction leads to severe acute respiratory failure. Surfactant deficiency causes respiratory distress syndrome (RDS) in preterm infants with immature lungs and surfactant dysfunction is important in the pathology of acute lung injury (ALI) and acute RDS (ARDS) in pediatric and adult patients [1, 25]. RDS is most prevalent in infants born at <32 weeks of gestation and affects about 40,000 preterm infants per year in the US. ALI/ARDS occurs in patients of all ages in association with direct and indirect lung injury [25, 26]. The complex pathophysiology of lung injury includes surfactant dysfunction, inflammation, vascular dysfunction, and cell/tissue injury [25–27]. Approximately 50,000–190,000 adults per year in the U.S. develop ARDS [26, 27], and the annual incidence of ALI is 22–86 cases per 100,000 adults [28, 29]. Children have a lower but still substantial incidence of ALI/ARDS of 2–12 cases per 100,000 per year [30]. Mortality rates for ALI/ARDS vary somewhat with specific etiology and patient population, but generally remain at high levels of 25–50% despite advanced medical intensive care. The important contribution of surfactant dysfunction to acute respiratory failure and ALI/ARDS provides a strong conceptual rationale for exogenous surfactant therapy in direct pulmonary forms of these syndromes in addition to neonatal RDS.

Clinical surfactant therapy for RDS was developed in the 1980s, primarily with animal-derived surfactant, and has greatly decreased the mortality and morbidity of preterm infants [31]. However, these native clinical surfactants are nontrivial in cost, and many very preterm infants with severe RDS still have impaired long-term outcomes due to progression towards bronchopulmonary dysplasia. At the introduction of lung surfactant replacement therapy, there was a fear for viral-induced and animal prion diseases, but none have been reported among the millions of preterm infants treated with animal-derived clinical surfactants. Surfactant therapy for ALI/ARDS is less developed than in the case of RDS, although benefits to respiratory outcomes and survival from surfactant administration have been documented in term infants with meconium aspiration and pneumonia, and in pediatric patients with direct ALI/ARDS [32]. Clinical studies of surfactant therapy in adults with ARDS have been more problematic. Two surfactant drugs, Exosurf® [33] and Survanta® [34], were tested in controlled trials in adults with sepsis-induced ARDS in the 1990's with little or no beneficial effects. However, Exosurf®, a mixture of DPPC and cetylalcohol and tyloxapol as spreading agents, is now known to have low surface activity and no longer used clinically, whereas the bovine-derived clinical surfactant Survanta® contains minimal levels of highly active SP-B [1].

It is important for surfactant therapy applications to distinguish between direct pulmonary causes of ALI/ARDS and systemic (indirect, nonpulmonary) causes. Indirect forms of ALI/ARDS frequently include multiorgan dysfunction and systemic inflammation not targeted by exogenous surfactants, making the therapy inherently less effective. Post hoc analyses in two trials have indicated significantly greater efficacy for exogenous surfactants in direct versus indirect forms of ALI/ARDS [35, 36]. The most positive placebo-controlled trial to date is the multicenter pediatric intensive care study of Willson et al. [35] with Infasurf®, a bovine-derived clinical surfactant that contains a substantial content of native SP-B and SP-C [1]. This multicenter trial in 153 pediatric patients demonstrated significant improvements in survival after tracheal instillation of Infasurf® in direct pulmonary forms of ALI/ARDS. These findings are consistent with extensive biophysical and animal studies indicating that surfactants with active protein/lipid compositions can reverse inhibitor-induced surfactant dysfunction and improve respiration if delivered effectively to the alveoli in direct lung injuries [25, 32]. Tracheal or bronchoscopic instillation as opposed to aerosolization is currently the most effective route of clinical surfactant delivery [1, 25, 32].

As pharmaceutical products, synthetic surfactants have significant potential advantages compared to animal-derived drugs in purity, reproducibility, quality-control, and scale-up economy compared to animal-derived preparations. The nontrivial batch-to-batch variability of animal-derived surfactants necessitates significant quality-control testing for composition and bioactivity. Synthetic drugs also have synthesis economies of scale not possible for animal products that have production costs directly proportional to animal usage. Synthetic surfactants are also free from the risk of prion-transmitted disease like bovine spongiform encephalitis, and are not subject to cultural and religious issues affecting bovine or porcine drugs in some countries. Components in synthetic surfactants can also be designed to have novel beneficial molecular properties for specific applications. One example of this is the use of phospholipase-resistant lipids in synthetic surfactants [37, 38]. Such surfactants are structurally resistant to degradation by endogenous phospholipases, which can be induced during the pulmonary inflammatory response in ALI/ARDS [39–41]. If ALI/ARDS is to be cost-effectively treated with surfactant therapy in pediatric and adult patients, recombinant or synthetic chemical drugs are far more likely to achieve this goal. The conceptual advantages of synthetic surfactants also potentially facilitate their utility and cost-effectiveness in other applications such as in the delivery of antibiotics or other drugs in liposomal systems.

Although the potential benefits of synthetic lung surfactant are clear, we should also be aware of potential limitations. We know relatively little about the metabolism and clearance of synthetic lung surfactant in the mammalian lung. We do know that native surfactant is cleared by alveolar macrophages and alveolar type 2 cells in the lung and that instillation of pure surfactant lipids (especially DPPC) does not lead to perturbation of the endogenous DPPC pool in the lung. However, there is only limited information about the metabolism of synthetic lung surfactant, i.e. surfactant composed of SP-B and/or SP-C mimics mixed in lipids, in the lungs. We have never recognized signs of toxicity from synthetic lung surfactants in animal experiments that lasted several hours, nor have other researchers reported toxicity in preterm lambs supported for 1–2 days after treatment with synthetic lung surfactant [42, 43]. Only 2 studies have investigated whether synthetic surfactant peptides affect alveolar type 2 cell function. Romero et al. [44] found that human alveolar type 2 cells and other lung cell types can incorporate the components of Surfaxin® (KL_4 surfactant) without altering the surfactant-related physiological functions of these cells. Poelma et al. [45] demonstrated that the uptake of liposomes with monomeric and dimeric SP-B(1–25) by alveolar type 2 cells was similar to the uptake of liposomes with native SP-B, but decreased by the addition of a mutant SP-B peptide. Similar studies should be done for the newer SP-B and SP-C peptides.

Synthetic Lipid/Peptide Lung Surfactant Design

The vast majority of synthetic lung surfactants are designed to incorporate, replicate, or substitute for functionally crucial molecular biophysical interactions present in native pulmonary surfactant. To accomplish this, synthetic surfactants typically require compositions containing both surface-active lipids and surface-active amphipathic peptides. Although native surfactant contains a broad mix of glycerophospholipid molecules, extensive research experience indicates that many of the functional biophysical characteristics of the overall phospholipid fraction can be replicated effectively by simpler compositions in synthetic surfactants (e.g., by DPPC plus a monounsaturated PC and/or PG component). By virtue of its saturated C16:0 chains, DPPC is extremely effective at lowering surface tension in dynamically compressed films at the air-water interface. The addition of a PC component acts to improve film fluidity and spreading during interfacial cycling, and the further addition of an anionic PG provides the potential for specific molecular interactions with cationic residues on surfactant peptides.

A similar conceptual strategy can be followed if novel phospholipase-resistant lipids are used rather than glycerophospholipids in synthetic lung surfactants. Highly active phospholipase-resistant synthetic surfactants have been prepared using DEPN-8, a C16:0 phospholipase-resistant diether phosphonate analog of DPPC [24, 37, 46]. The saturated fatty chains and large zwitterionic headgroup of DEPN-8 give it strong surface tension lowering power in analogy with DPPC, while its ether linkages increase film fluidity and spreading facility compared to ester-linked DPPC [24, 37, 46]. This makes it unnecessary to include an added unsaturated PC in synthetic surfactants containing DEPN-8, although an added PG analog can again be used to provide for specific molecular interactions with cationic residues on surfactant peptides [38].

The most challenging chemical components of synthetic surfactants are those mimicking the activity of native lung SPs. Major interest focuses on components related to SPs SP-B and SP-C, since they are present in animal-derived surfactant drugs that have documented clinical benefits in preterm infants. In contrast, hydrophilic SP-A protein is removed during organic solvent extraction or column chromatographic processes used in preparing all current animal-derived surfactant drugs. SP-B is the most active and physiologically pivotal of all the native SPs [1, 2]. Extensive laboratory studies have documented that SP-B is more active than SP-C in interacting biophysically with lipids in lung surfactant activity [47], and supplementation with SP-B or synthetic SP-B peptides increases the activity of surfactants containing only SP-C in animal models [48]. Knockout mice with isolated SP-B deficiency die shortly after birth of respiratory failure [49], and human infants with SP-B mutations do not survive beyond the first days of life without surfactant replacement (and ultimately lung transplantation) [50, 51]. Experiments by Ikegami et al. [52] using conditional knock out mice showed that adult animals rendered acutely deficient in SP-B developed severe respiratory distress with surfactant dysfunction and pulmonary inflammation. Mice left SP-B deficient died with pathology resembling ARDS, but the abnormalities were reversed and the mice survived if SP-B synthesis was restored. All mice maintained normal levels of SP-C during study [52].

The remainder of this article focuses on the design and synthesis of SP-B peptides, and their use in highly active synthetic lung surfactants. First, descriptions are presented of MB and S-MB, two highly active SP-B peptides synthesized and studied in our laboratories [14, 24]. These are followed by an overview of strategies for developing new SP-B peptides via molecular design.

MB and S-MB Synthetic Peptides

Synthetic Peptides Based on the N- or C-Terminal Domains of SP-B Fold as α-Helical, Amphipathic Domains and Exhibit Surfactant Activities

Early homology models of SP-B, in which the primary sequence of SP-B was templated on the known 3D structure of NK-lysin, granulysin, and saposins A, C, and D indicated that SP-B may fold as a closed saposin (see above; Fig. 1) [12–14]. Circular dichroism and FTIR spectroscopy of full-length SP-B confirmed the high α-helical content predicted by these homology models [53, 54]. To test the hypothesis that the exposed N- and C- terminal helical domains of native SP-B (i.e., the N-terminal insertion sequence and helix 1 and C-terminal helix 5 of Fig. 1) may promote surfactant activity, synthetic peptides encompassing each of these regions were previously investigated in structural and functional studies. Based on the human SP-B sequence (SP-B residues 1–25: FPIPLPYCWLCRALIKRIQAMIPKG), residue-specific ^{13}C-FTIR spectroscopy of synthetic SP-B(1–25) (PDB accession code: 1DFW; www.rcsb.org) [18] or 2D-NMR spectrometry on synthetic SP-B(11–25) (PDB: 1KMR) [20] verified the N-terminal α-helix (~residues 10–20) predicted in the above 3D-homology models for SP-B (Fig. 1). Prior physical experiments indicated that the helical N-terminal region of SP-B(1–25) anchors this peptide onto lipids, such that the long molecular axis lies at an oblique angle to the lipid bilayer plane with the neutral and charged residues oriented towards the polar headgroup region and the hydrophobic residues directed towards the lipid acyl chains [17]. Importantly, SP-B(1–25) and full-length SP-B each increased the collapse pressure of lipid monolayers containing palmitic acid. The cationic N-terminus of SP-B may here interact with anionic lipids to remove the driving force for lipid squeeze-out from the surface film [55, 56]. In further studies, SP-B(1–25) and native SP-B each induced a coexistence of buckled and flat monolayers when added to surfactant lipids, promoted a low surface tension and increased respreading of the surfactant monolayer [57]. Follow-up investigations using atomic force microscopy demonstrated that the molecular topography of surfactant lipid films containing SP-B(1–25) has extensive "nanosilo" formation (i.e., large cylindrical multilayer stacks of lipid-peptide ensembles 200–400 nm in diameter and 20 nm in height attached to the surface monolayer) as a function of surface pressure [58]. The above in vitro surfactant activities of SP-B(1–25) are also correlated with the improved oxygenation and lung compliance noted for this peptide in surfactant-deficient animal models [59–62]. Because physical studies indicated high α-helical levels for N-terminal SP-B peptides in lipids or membrane-mimics [17, 18, 20, 63, 64], the N-terminal domain in native SP-B may contribute to surfactant actions as a charged amphipathic α-helix.

Peptides encompassing the C-terminal region of native SP-B (i.e., the C-terminal helix 5 in Fig. 1) may also participate in lung surfactant activities. Similar to the N-terminal domain, the positively charged helical C-terminus of SP-B may be involved in lung functions, as synthetic peptides either directly (e.g., SP-B residues 63–78: GRMLPQLVCRLVLRCS) (PDB: 1RG3, 1RG4) or indirectly (e.g., KL4 [21 residues]: KLLLLKLLLLKLLLLKLLLLK) representing the C-terminus may adopt helical conformations [22, 65–67] and promote in vitro [65, 66, 68, 69] and in vivo [68, 70, 71] surfactant activities mimicking those of the native protein. Importantly, lucinactant, a new total synthetic lipid-peptide preparation that includes the KL4 peptide designed to loosely mimic the C-terminal domain of SP-B, has been tested in two clinical trials with preterm infants at risk for RDS [72, 73]. Lucinactant (Surfaxin®) contains a mixture of lipids and the sinapultide peptide, also known as KL4 because of its repeating motif of one lysine followed by four leucine residues (see above). These infant studies indicated positive results [72, 73], and the Food and Drug Administration (FDA) approved Surfaxin® in 2012 for the clinical treatment of RDS. Surfaxin® was the first approved therapy in the US that treats a surfactant deficiency with a total synthetic lipid-peptide formulation,

and represents a new class of synthetic surfactants containing lipids and limited quantities of SP-B and/or SP-C mimics. Despite this important advance, however, there were problems in the storage and delivery of Surfaxin®. The above clinical trials indicated that Surfaxin® forms a gel in its storage form, and must first be heated to 44°C and then shaken before tracheal administration. The physical basis for this gel formation is not yet known, but may be related to the low binding of KL4 to lipids when compared to native SP-B and SP-C [70], and also to the ability of KL4 to form both β-sheet and α-helix with either mixed lipid monolayers [74] or mixed liposomes at high peptide loading [75]. Such stability problems limited the widespread use of Surfaxin® in the treatment of surfactant deficiencies, particularly in emergencies, and have led to the voluntary decision by its producer to withdraw Surfaxin® from the market in 2015.

Design of Advanced MB and S-MB Peptides to More Closely Mimic Key Structural and Functional Properties of Full-Length SP-B

Although peptides directly representing the N- or C-terminal domains demonstrate significant in vitro and in vivo surfactant functions (see above), these synthetic peptides, when tested alone or in combination, show substantially lower surfactant activities than those of native SP-B [14]. The above results suggest that the topographical organization of the N- and C-terminal helical domains in full-length SP-B may play a critical role in the expression of high surfactant activities. In this context, the homology model for SP-B (Fig. 1) indicates that the N-terminal insertion sequence and helix 1 (SP-B residues 1–25) and the C-terminal helix 5 (SP-B residues 63–78) will constitute one of the two "leaves" of SP-B, in which the N- and C-terminal helices are neighboring amphipathic α-helices with the disulfide cross-links (i.e., Cys-8 to Cys-77 and Cys-11 to Cys-71; numbering from full-length SP-B) locking in this close juxtaposition. Novel SP-B mimics have accordingly been designed to more closely reproduce the topology of the N- and C-terminal motifs of the parent protein. One such SP-B mimic developed by our group is *Mini-B* (MB [residues 8–41]: CWLCRALIKRIQAMIPKG-GRMLPQLVCRLVLRCS; numbering according to the below S-MB), a 34-residue peptide that incorporates residues 8–25 and 63–78 of native SP-B as a single linear peptide. MB is a truncated or "short-cut" version of SP-B, with the N-terminal insertion sequence (SP-B residues 1–7: FPIPLPY) omitted and helices 2–4 (i.e., SP-B residues 26–62) (Fig. 1) replaced with the four-residue (PKGG) sequence. The hydrophilic PKGG sequence would likely participate in an MB turn, as earlier proteomic surveys indicated that turns are primarily composed of hydrophilic residues such as glycine and proline [76]. Furthermore, previous theoretical predictions using neural network algorithms indicated that the PKGG sequence in MB will fold as a β-turn [77, 78]. The designer helix – β-turn – helix structure in MB would be expected to bring the two helices into close juxtaposition, thereby permitting the formation of disulfide bridges between Cys-8 and Cys-77, and also between Cys-11 and Cys-71.

Because prior results with SP-B peptides [17, 18, 58, 63, 79, 80] suggested that the N-terminal sequence (i.e., residues 1–7) plays key roles in the surfactant properties of full-length SP-B, we next engineered the *Super Mini-B* (S-MB), a 41-residue peptide mimic in which residues 1–7 were covalently attached to the N-terminus of MB (S-MB [residues 1–41]: FPIPLPYCWLCRALIKRIQAMIPKGGRMLPQLVCRLVLRC). S-MB might be expected to show higher surfactant activity than MB, because the former peptide may more accurately mimic the leaflet structure containing the N- and C-terminal domains of SP-B (Fig. 1). Neural network algorithms also predict that the presence of the N-terminal insertion sequence in S-MB will not influence the ability of PKGG to fold as a β-turn [77, 78]. Interestingly, the N-terminal XPXPXPY motif, where X denotes hydrophobic residues, may serve as a lipid insertion sequence to more firmly anchor S-MB to lipid monolayers and bilayers, as has been experimentally observed for the N-terminal SP-B(1–25) peptide [17]. Moreover, the N-terminal

insertion sequence (residues 1–7) for S-MB may facilitate the production of noncovalently associated S-MB dimers (see below), and this in turn may influence the lipid-binding properties of S-MB.

Synthesis of MB and S-MB as Saposin (SP-B) Mimic Peptides

MB and S-MB were synthesized on a Symphony Multiple Peptide Synthesizer (Protein Technologies, Tucson, AZ, USA) using a FastMoc™ protocol [81] on a H-Serine (OtBu) HMPB NovaPEG resin (NOVAbiochem, Billerica, MA, USA) [14, 19, 24]. All residues are double-coupled to the resin to ensure optimal yield. After cleavage and deprotection [14], crude peptides are separated from the resin by filtration, dissolved in trifluoroethanol:10 mM HCl (1:1, v:v), and freeze-dried to uniform powders that can easily be dissolved in organic solvents for further purification (>95%) by preparative HPLC and mass confirmation by MALDI TOF mass spectrometry. Folding of HPLC-purified, reduced peptides into disulfide-linked helical structures closely resembling the saposin fold of native SP-B is then facilitated by specific solvents [14, 82, 83]. Following oxidation, final MB and S-MB peptides are re-purified by reverse-phase HPLC using the same boundary conditions as employed for the crude material [14, 19, 24, 83]. This allows separation of any residual reduced peptide away from desired final oxidized product peptides. The molecular mass of oxidized MB and S-MB is then re-checked by mass spectroscopy, and disulfide connectivity confirmed by mass spectroscopy of enzyme-digested fragments (trypsin and chymotrypsin digestion). After dialysis, the purified, desalted peptides can be freeze-dried to give a uniform powder for combination with lipids in synthetic surfactants [14, 19, 24, 83].

^{12}C-FTIR Spectroscopic Analysis of MB and S-MB in Lipid-Mimic and Lipid Environments

To assess whether MB and S-MB adopt the helix-turn-helix conformation predicted by homology modeling, FTIR spectra were obtained for these peptides in lipid mimic and lipid environments [19]. FTIR spectra of the amide I band for MB in these environments (Fig. 2a) were all similar, indicating that MB peptide adopts multiple conformations with a major component centered at ~1,657–1,651 cm^{-1} (α-helix) and minor components centered at ~1,620 cm^{-1} (β-sheet) and 1,682–1,660 cm^{-1} (β-turns). Self-deconvolutions of the Figure 2a spectra confirmed that MB is comparably polymorphic in each of these milieus, essentially sharing the following relative proportions of secondary structure: α-helix (35–47%) > β-sheet (15–24%) ~ loop-turn (8–25%) ~ random (20–24%). FTIR spectra obtained for S-MB (Fig. 2b) were similar to the corresponding MB spectra in Figure 2a. Deconvolution of these S-MB spectra confirmed elevated levels of α-helix (30–39%), with smaller amounts of β-sheet (19–27%), loop-turn (24–29%) and random (9–21%) structures. These FTIR spectra suggest that oxidized MB and S-MB both fold with the disulfide-linked, helix-turn-helix structure predicted by homology modeling, that their secondary conformations are remarkably stable in a wide range of lipid and lipid-mimic environments, and that incorporation of the N-terminal insertion sequence in S-MB does not grossly perturb the helical core shared by MB and S-MB [19].

Residue-Specific Determinations of the MB Structures Using ^{13}C-FTIR or 2D-NMR Spectroscopy

Although the above ^{12}C-FTIR results are consistent with oxidized MB folding as a helix-turn-helix, this spectroscopic technique cannot attribute secondary conformations to specific amino acid residues. To more precisely identify secondary structures within oxidized MB, ^{13}C-FTIR spectroscopy was performed with site-directed, isotope-enhanced peptides and indicated that the oxidized peptide folded its N- and C-terminal domains as α-helices, with a β-conformation (i.e., encompassing –PKGG–) connecting the neighboring helices [14].

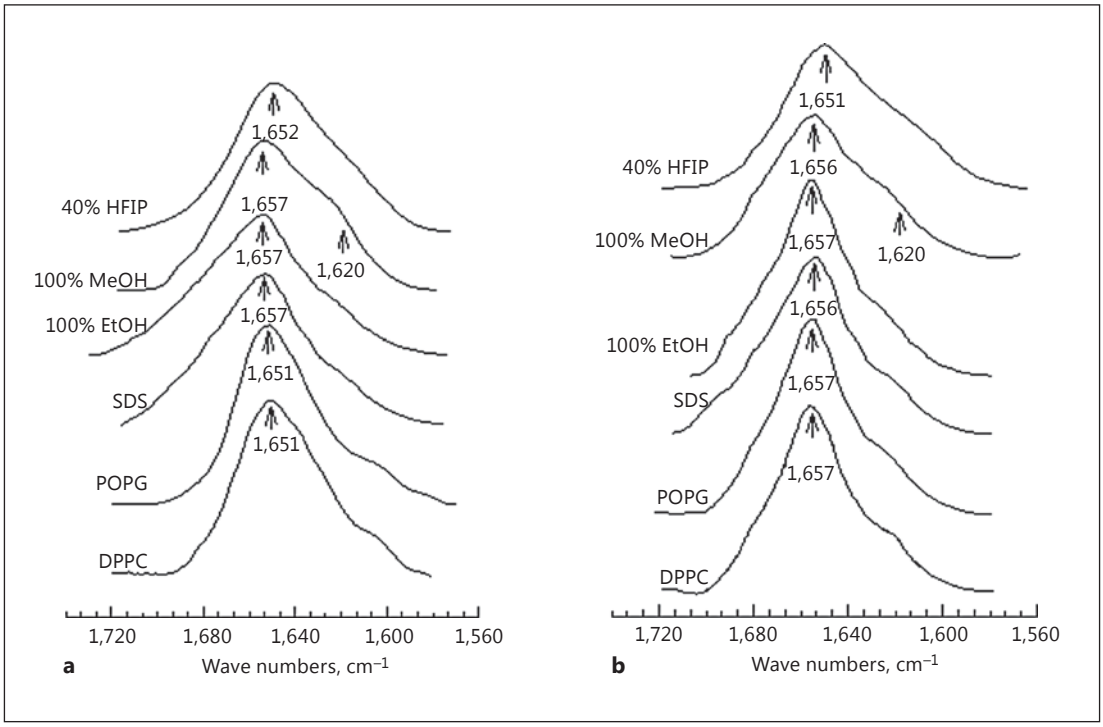

Fig. 2. FTIR spectra of MB and S-MB in the structure-promoting solvents hexafluoroisopropanol (HFIP), methanol (MeOH) and ethanol (EtOH), the detergent SDS (sodium dodecyl sulfate), and the phospholipids POPG and DPPC. Methanol and ethanol are solvents of intermediate polarity that mimic the polar head group domain of phospholipid bilayers, while HFIP represents the more hydrophobic interior of the lipid bilayer. **a** Stacked FTIR spectra of MB in 40% HFIP (i.e., 40% HFIP/60% deuterated-sodium phosphate buffer, pH 7.4), 100% MeOH (i.e., 100% methanol), 100% EtOH (i.e., 100% ethanol), SDS, POPG, and DPPC. **b** Stacked FTIR spectra of S-MB in 40% HFIP, 100% MeOH, 100% EtOH, SDS, POPG, and DPPC. **a**, **b** The IR spectra for MB and S-MB each show dominant α-helical components centered at 1,657–1,651 cm^{-1} (arrows), with minor bands at ~1,637–1,613 cm^{-1} (arrow at 1,620 cm^{-1}) denoting β-sheet. Peptide concentrations were 470 μM for solvent spectra and 10:1 lipid:peptide (mole:mole) for lipid spectra. The abscissa (left to right) is 1,740–1,560 cm^{-1}, while the ordinate represents absorption (in arbitrary units).

Molecular dynamics (MD) simulations confirmed that oxidized MB folds as a globular bundle, consisting of adjacent N- and C-terminal α-helices connected by a β-turn at –PKGG– and cross-linked by disulfides (see PDB: 1SSZ, www.rcsb.org; Fig. 3a). The MB backbone folding in the lipid mimic hexafluoroisopropanol (HFIP) (Fig. 3a) closely overlaps the corresponding domains of homology-modeled SP-B (Fig. 1). Thus, oxidized MB faithfully reproduces the topographical organization of the saposin leaf containing the N- and C-terminal helical domains in full-length SP-B (Fig. 1) [14], and the designer –PKGG– sequence of MB accommodates the close approach of these helical regions to form intrachain disulfide bridges [14].

More recently, 2D-NMR spectroscopy has elucidated the 3-D structure of reduced MB in an HFIP solution, and that of oxidized MB in sodium dodecyl sulfate detergent micelles [21]. Similar to that noted above for oxidized MB (1SSZ) in HFIP, 2D-NMR analysis showed that the N- and C-terminal regions of reduced MB in HFIP (PDB: 2JOU) fold as α-helices (Fig. 3a, b). However, reduced MB in HFIP (Fig. 3b) is unable to form the characteristic helix-turn-helix of oxidized MB, instead folding as a linear peptide with the N- and C-terminal helices at opposite ends (Fig. 3a). These findings support our earlier MB experiments (see Synthesis of

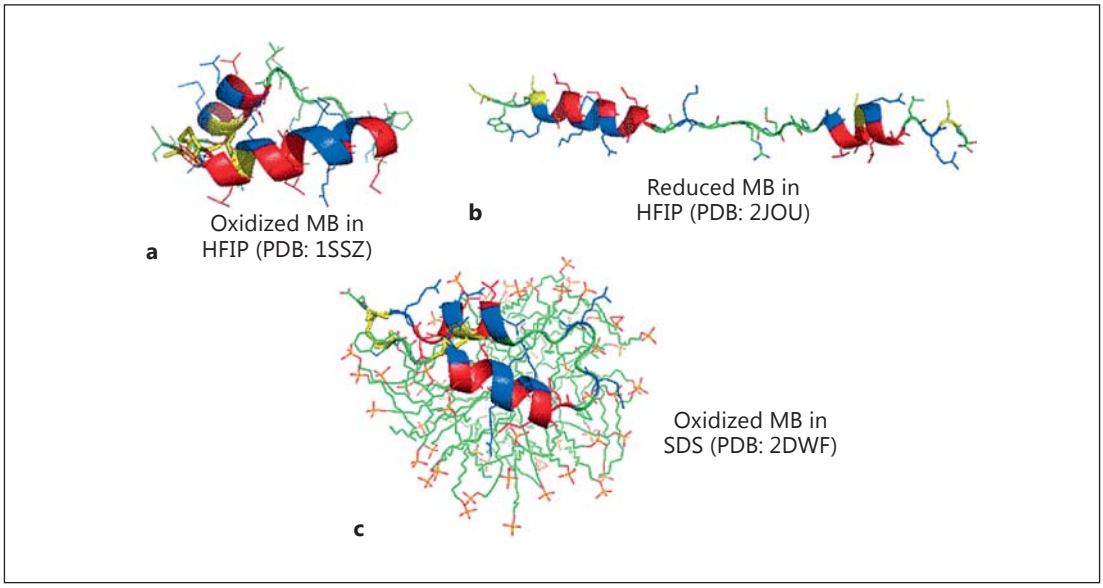

Fig. 3. Residue-specific 3D structures for Mini-B (MB) in either HFIP solutions (**a**, **b**) or SDS micelles (**c**) determined using ^{13}C-FTIR or 2D-NMR spectroscopy. PyMOL representations of peptide backbones are shown as either thick (N- and C-terminal α-helices) ribbons or thin green (turn regions) ribbons; amino acid sidechains are represented as wireframes. Polar residues are colored blue, with nonpolar and cysteine residues in red and yellow, respectively. **a** The ^{13}C-FTIR structure for oxidized MB, disulfide-linked at Cys-8 to Cys-40 and Cys-11 to Cys-34 (see bottom left; S-MB numbering) (PDB Accession Code: 1SSZ). The β-turn connecting the N-terminal (foreground) and C-terminal (background) α-helices is shown in green. **b** The 2D-NMR structure for reduced MB with no disulfide-links and the Cys-8 on the left and the Ser-41 on the right (PDB: 2JOU). **c** The 2D-NMR structure for oxidized MB with disulfide links associated with an SDS micelle; SDS molecules are modeled as stick figures, with their fatty acyl groups in green and polar headgroups in red (PDB: 2DWF). The N- and C-terminal helices of oxidized MB in either **a** or **c** reproduce the folding of these domains in homology-modeled SP-B (see Fig. 1).

MB and S-MB as Saposin (SP-B) Mimic Peptides) indicating that only certain solvents with high turn propensities (e.g., trifluoroethanol buffer solutions) are able to position the N- and C-terminal helices close enough to form intrachain disulfide bonds. Once the proper disulfides are formed, oxidized MB adopts a stable helical bundle that is effectively *stapled* by the covalent-linkages between neighboring Cys residues. The N- and C-terminal helical axes are nearly parallel for oxidized MB when bound to sodium dodecyl sulfate micelles (Fig. 3c), while the corresponding axes tilt at an acute angle for oxidized MB in HFIP (Fig. 3a). The peptide backbone of oxidized MB (PDB: 2DWF) closely overlapped the N- and C-terminal domains of experimentally determined saposins in both the *open* and *closed* states, confirming that MB is a general mimic for saposin leafs containing the N- and C-terminal helices [21].

MD Simulations of MB and S-MB in Lipid-Mimic and Lipid Environments

MD simulations were conducted to assess residue-specific conformations for MB and S-MB in both lipid-mimics and surfactant lipids [19]. MD simulations for the oxidized MB in 40% HFIP/60% water indicated that the characteristic helix-turn-helix motif was strongly conserved throughout the duration of the run (0–100 ns). The "0 ns" model for oxidized MB in HFIP is virtually indistinguishable from the 1SSZ structure on which it is based (Fig. 3a) and is folded as a helix-hairpin-helix when stabilized by disulfide linkages [19]. The axes of

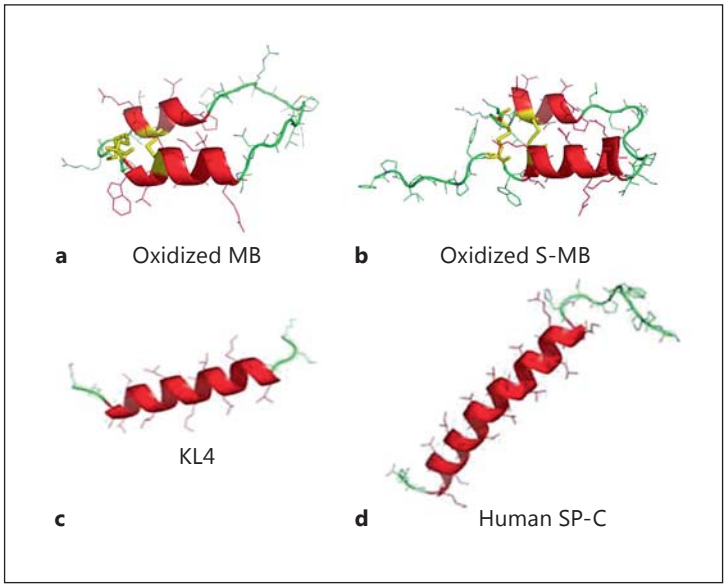

Fig. 4. Comparison of the 3D-structures for Mini-B (MB) (**a**) and Super Mini-B (S-MB) (**b**) in 40% HFIP/60% water determined using molecular dynamics (MD) simulations with preliminary 3D models for KL4 (**c**) and human SP-C (**d**). PyMOL representations of backbones are shown as either thick (N- and C-terminal α-helices) ribbons or thin green (extended or turn regions) ribbons; side chains are represented as wireframes. **a** MD simulation of MB in 40% HFIP/60% water at 100 ns, with the linked Cys-8 and Cys-40 and Cys-11 and Cys-34 (yellow) at the lower left and the turn region (PKGG in green) at the upper right. The N-terminal helix is in the foreground and the C-terminal helix is in the background, with the helical axes nearly parallel. **b** MD simulation of S-MB in 40% HFIP/60% water at 100 ns, with the extended N-terminal insertion sequence (residues 1–7) in an extended conformation (green) at the lower left and the turn region (PKGG; green) at the upper right. The linked Cys-8 and Cys-40 and Cys-11 and Cys-34 (yellow) are adjacent to the insertion sequence. The N-terminal helix (red ribbon) is in the foreground, and the C-terminal helix (red ribbon) is in the background, with nearly parallel helical axes. **c** Model of the 21-residue KL4 as an α-helix, with residues 2–20 folding as an α-helix (red ribbon) (see the sections Synthetic Peptides Based on the N- or C-Terminal Domains of SP-B Fold as α-Helical, Amphipathic Domains and Exhibit Surfactant Activities and MD Simulations of MB and S-MB in Lipid-Mimic and Lipid Environments). **d** Homology model for the 35-residue human SP-C, in which the human sequence is templated onto the 2D-NMR structure of the porcine SP-C (PDB: 1SPF) (see text). The homology-modeled human SP-C folds as an α-helix (red ribbon) for residues 9–33, with residues 1–8 and 33–35 forming extended conformations (green ribbons). Leu-35 is at the lower left, while the N-terminal Leu-1 is at the upper right (see the section MD Simulations of MB and S-MB in Lipid-Mimic and Lipid Environments).

the N- and C-terminal helices in the "0 ns" model are tilted at an angle [19] comparable to that seen in the 1SSZ structure [14]. At the end of the MD simulation, the final "100 ns" model for oxidized MB in HFIP (Fig. 4a) indicates that the major conformational elements of the original 1SSZ structure are largely conserved. Specifically, Figure 4a shows that the "100 ns" MB structure is a disulfide-linked bundle containing N- and C-terminal helices with nearly parallel axes, which also exhibits considerable interactions between hydrophobic side chains across the interhelix interface.

Comparable MD simulations were next carried out on the pre-equilibrated "0 ns" model for oxidized S-MB in 40% HFIP/60% water. The final "100 ns" S-MB structure (Fig. 4b) demonstrated a helix-turn-helix motif, which closely matches the secondary structure and overall topography of the "100 ns" MB structure, and indicates that the N-terminal insertion sequence in S-MB exerts minimal influence on the final organization of the helical core [18].

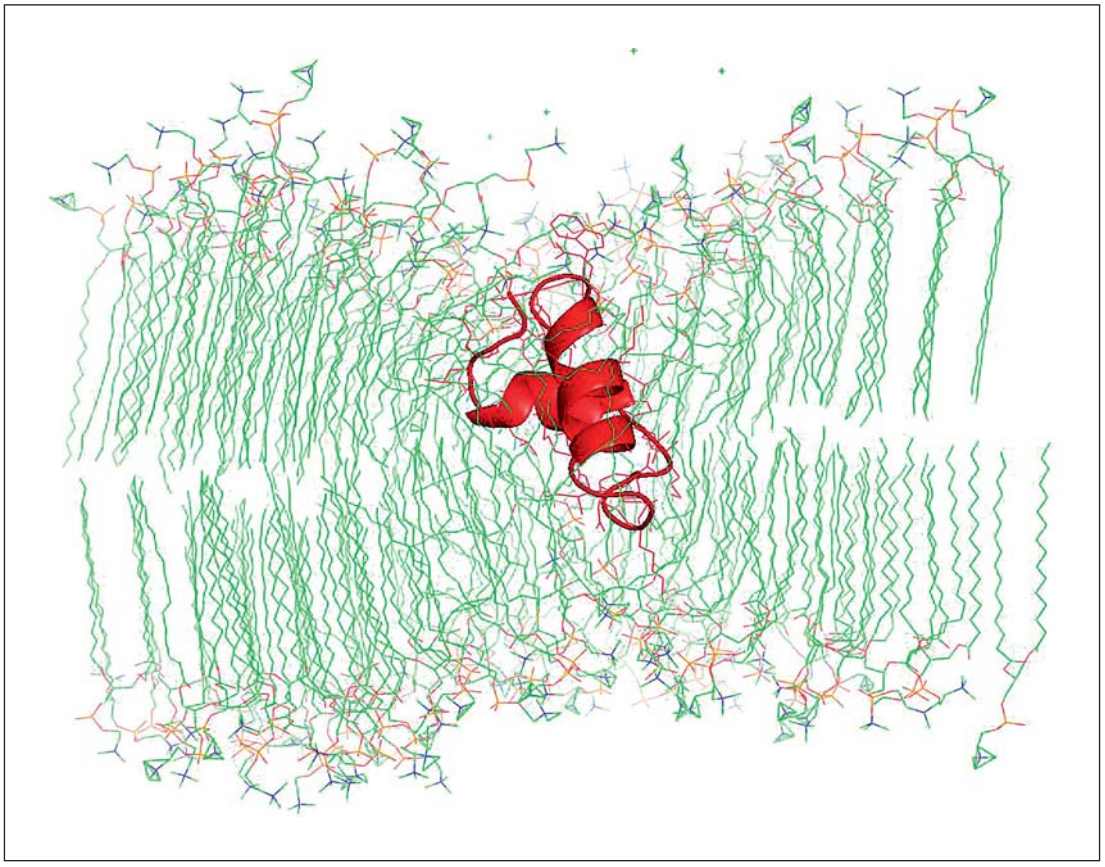

Fig. 5. Cross-sectional view of the insertion of the Mini-B (MB) peptide into bilayers of dipalmitoyl phosphatidylcholine (DPPC) after 100 ns of molecular dynamics (MD) simulations. The MB peptide backbone is shown in red highlight, with the N- and C-terminal α-helices modeled as thick ribbons. The zwitterionic DPPC lipids are modeled as stick figures, with the hydrophobic fatty acyl chain in green and the polar head group region containing the anionic phosphate group in red, and the cationic choline group in blue. Docking of MB into the DPPC bilayer and subsequent MD simulations were performed as described in the section MD Simulations of MB and S-MB in Lipid-Mimic and Lipid Environments.

The N-terminal sequence (Phe-1 to Pro-6) of S-MB adopts a random coil conformation in the "100 ns" model, probably due to its repeated proline motif that prevents back H-bonding to form intramolecular β-turns and/or β-sheets.

Although the above computer simulations were limited to MB and S-MB in lipid-mimetic solvents, more relevant 3D-structures may be obtained by performing MD simulations on these peptides in surfactant lipids. For "100 ns" of MD simulations, Figure 5 shows a cross-sectional view of the oxidized MB peptide bound to the polar headgroup region of the DPPC lipid bilayer. Here, MB retains its characteristic helix-turn-helix conformation, with the axes for both the N-terminal and C-terminal helices at an oblique angle with respect to the membrane plane.

It is worthwhile comparing the structural properties of the above MD-simulated MB and S-MB peptides with those of the related surfactant peptides KL4 and SP-C (Fig. 4). As noted earlier, Surfaxin® has recently been approved in the US by the FDA for treatment of neonatal RDS, and contains the 21-residue KL4 as its surfactant-active peptide component. KL4 is loosely based on the C-terminal sequence of SP-B (i.e., SP-B residues 63–78 or MB/S-MB

residues 26–41 [19]), and shows surfactant activity when folded as an α-helix (Fig. 4c). Several mechanisms have been proposed to account for the surfactant activities of KL4, ranging from an "SP-B-like" model [58, 84] to one similar to that of the transmembrane helical SP-C [85, 86] (Fig. 4d), but none has yet gained general acceptance. SP-C is a short 35-residue hydrophobic protein in human lungs with a relatively unstructured N-terminus (residues 1–8) with residues 9–34 forming a stable α-helix in the mid- and C-terminal regions (PDB: 1SPF). When incorporated into lipids, FTIR spectroscopy has shown that SP-C is principally α-helical, with its long molecular helix axis parallel to the phospholipid acyl chains, and it is widely accepted that SP-C mediates its surfactant activities in the lung by folding as a transmembrane α-helix [13, 23, 87].

Self-Association Properties for MB and S-MB Peptides

Native SP-B functions as a homodimer, and we therefore assessed the self-association propensities of the oxidized MB and S-MB peptides. Molecular weight and aggregation analyses performed with SDS-PAGE indicated only monomers for MB, while S-MB readily formed dimers with a minimal presence of monomers; no evidence for higher-order oligomers was observed for either MB or S-MB [19]. Furthermore, surface plasmon resonance sensorgrams demonstrated high self-association for S-MB, but much lower self-association for MB [19]. Because the N-terminal sequence Phe-1 to Tyr-7 is present in S-MB but not in MB, the increased dimers in S-MB may be due to the N-terminal insertion sequence promoting intermolecular β-sheet formation between S-MB monomers. The respective MB and S-MB sequences were analyzed with PASTA to assess those regions most likely to form β-sheet, particular in polar environments such as in aqueous buffer or at the lipid-water interface (http://protein.cribi.unipd.it/pasta; [88, 89]). The most stable β-sheet for all of the MB and S-MB pairings analyzed with PASTA was an antiparallel β-sheet pairing for S-MB (i.e., N-terminal Tyr-7 to Arg-12 strand), suggesting that the dimeric S-MB observed experimentally [19] might be due to two antiparallel S-MB monomers forming β-sheet at this aggregation "hot spot." The above prediction for the structure of dimer S-MB was confirmed in silico using homology modeling, molecular docking [90, 91], and MD simulations.

Surface Activity of Synthetic Lipid/Peptide Lung Surfactants Containing MB and S-MB Peptides

The beneficial molecular properties of MB and S-MB peptides correlate directly with high surface activity when these peptides are combined with lipids in synthetic lung surfactants. Plasmon resonance spectroscopic data showed that both MB and S-MB have a high molecular affinity for lipids, such as DPPC and DEPN-8, with S-MB peptide having the greatest molecular affinity of the two peptides. Measurements of the surface activity of synthetic surfactants containing S-MB, MB, or purified porcine SP-B combined with lipids were made on a captive bubble surfactometer originally defined by Schurch et al. [92, 93] (Fig. 6). Captive bubble surfactometry provides a physiologically relevant assessment of overall surface activity that reflects a combination of adsorption, dynamic film compression, and dynamic film spreading at physical conditions similar to those at the alveolar interface in vivo at 37°C [92, 93]. Lipids used in the synthetic surfactants were phospholipase-resistant DEPN-8 or one of two mixtures of standard glycerophospholipids that roughly reflected the mix of lipid classes found in endogenous surfactant (DPPC:POPC:POPG:POPE:cholesterol 8:5:3:0.5:1 or DPPC:POPC:POPG 5:3:2 by weight) [94]. Synthetic surfactant preparations included 1.5% (or higher) of S-MB or MB in standard glycerophospholipids or 1.5% of MB in DEPN-8. Purified porcine SP-B in standard glycerophospholipids and Infasurf® were studied as a positive controls, while glycerophospholipids (lipids alone) served as a negative control. Synthetic glycerophospholipid/S-

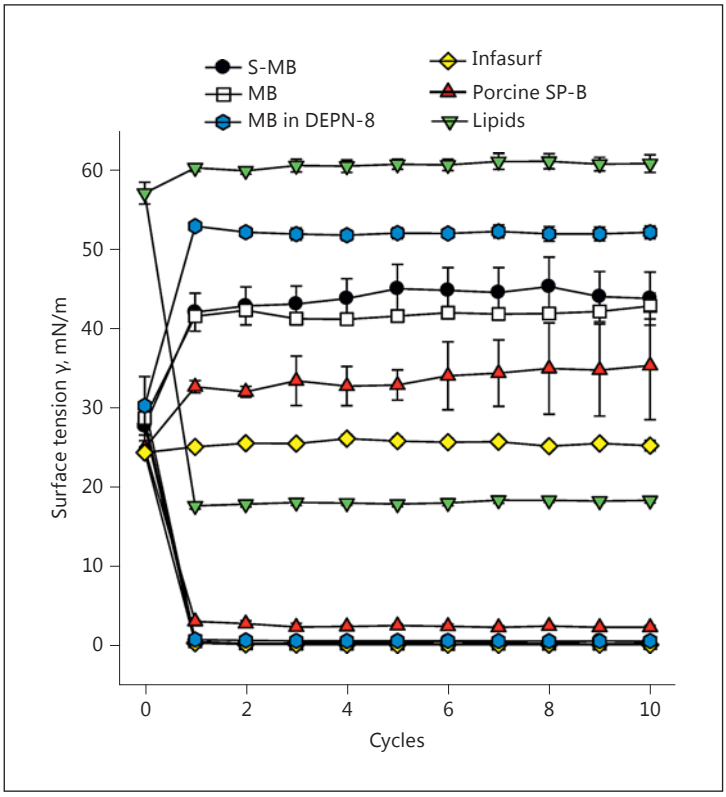

Fig. 6. Surface activity of synthetic lung surfactants measured with captive bubble surfactometry. Surface activity of synthetic lung surfactants was studied with a captive bubble surfactometer at 37°C. Synthetic surfactant preparations included Super Mini-B (S-MB) formulated with standard glycerophospholipids (DPPC:POPC:POPG 5:3:2 by weight) and Mini-B (MB) formulated with glycerophospholipids or the phospholipase-resistant lipid DEPN-8. Porcine SP-B in standard glycerophospholipids and Infasurf®, a bovine-derived clinical surfactant with both SP-B and SP-C, were studied as positive controls, while glycerophospholipids alone served as a negative control. Synthetic glycerophospholipid/peptide and DEPN-8 surfactants were all highly active in reducing minimum surface tension to ≤1 mN/m on the captive bubble surfactometer throughout 10 consecutive quasi-static compression-expansion cycles. Data are mean ± SEM for n = 4–8.

MB or MB or SP-B surfactants, DEPN-8/MB surfactant, and Infasurf® were all highly active in reducing minimum surface tension to ≤1 mN/m on the captive bubble surfactometer throughout 10 consecutive quasi-static compression-expansion cycles.

Pulmonary Activity of Synthetic Lipid/Peptide Surfactants Containing MB/S-MB Peptides

The pulmonary activity of synthetic surfactants containing surfactant lipids plus at least 1.5% of S-MB or MB was assessed in mechanically-ventilated, lung-lavaged rats as a rodent model relevant for both RDS and ALI/ARDS. The activity of Infasurf® and purified porcine SP-B surfactant was also examined as a positive control, and lipids alone were used as a negative control. Infasurf® has been documented previously to improve survival and respiratory function in preterm infants with RDS [95] and in children with ALI/ARDS [35]. Complete methods for in vivo lavage, mechanical ventilation, and experimental assessments of oxygenation and dynamic compliance in this rat model have been detailed previously [14, 19, 48, 60, 62, 94]. In brief, rats were anesthetized, intubated, and vascular catheters were inserted. Gentle lavage of the lungs (typically 8 lavages with 8 ml of normal saline) was done with animals

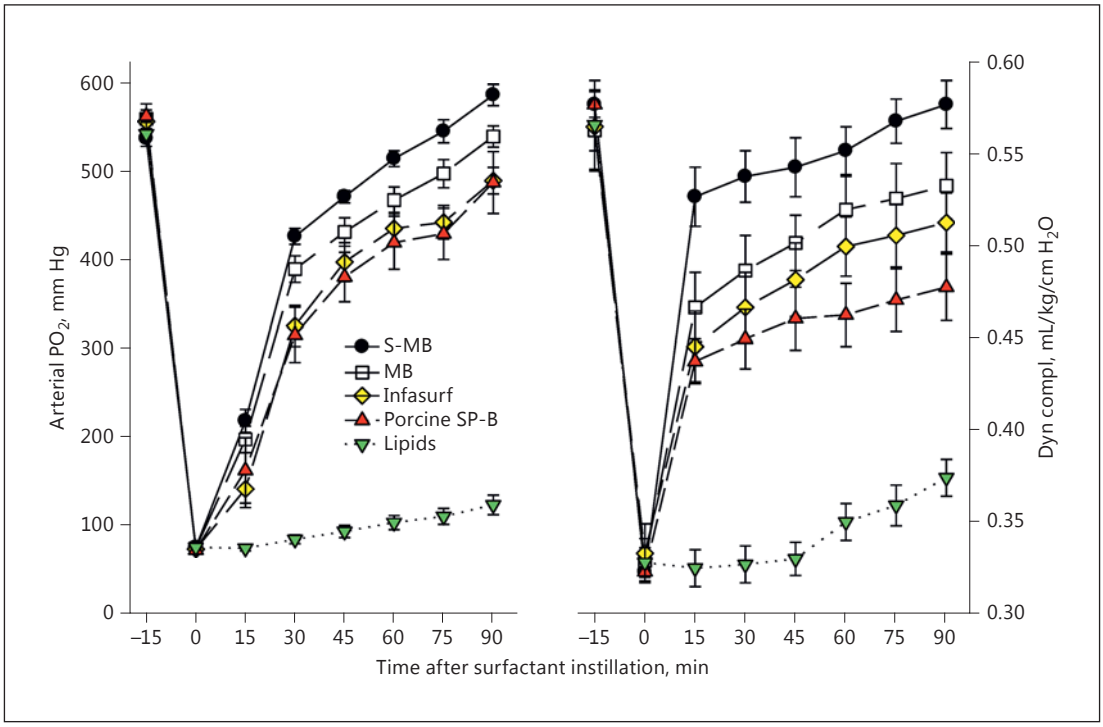

Fig. 7. Improved oxygenation and dynamic compliance in ventilated, lung-lavaged rats in vivo following the instillation of various synthetic lung surfactants. Surfactants (100 mg/kg) were instilled intratracheally into mechanically ventilated adult rats following in vivo lavage to reduce PaO_2 in 100% oxygen to <100 mm Hg, consistent with clinical ARDS (see Pulmonary Activity of Synthetic Lipid/Peptide Surfactants Containing MB/S-MB Peptides for animal model details). Synthetic surfactant containing surfactant lipids plus Super Mini-B (S-MB) peptide had the greatest activity in improving oxygenation and compliance, followed by an analogous surfactant containing Mini-B (MB). Porcine SP-B in surfactant lipids and Infasurf®, a bovine-derived clinical surfactant with both SP-B and SP-C, were studied as positive controls, while surfactant lipids alone served as a negative control.

breathing 100% oxygen until PaO_2 was stable and less than 100 mm Hg (well within the oxygenation range of clinical ARDS). An exogenous surfactant was then instilled intratracheally (100 mg/kg body weight in 35 mg/ml dispersions) and the animals ventilated with 100% oxygen with a Harvard volume-controlled small animal ventilator. Ventilation was monitored continuously, and arterial pH and blood gases were assessed every 15 min along with dynamic compliance. Anesthesia was maintained throughout, and rats were sacrificed at 90 min after surfactant administration. Results showed that S-MB surfactant had very high activity in increasing arterial oxygenation, exceeding the activity of Infasurf® (Fig. 7). MB surfactant was also very active in improving oxygenation in these rat studies, but did not reach the level of S-MB surfactant. The various surfactants had the same order of effectiveness in increasing dynamic compliance or lung volumes at fixed pressure (i.e., S-MB > MB > Infasurf® > porcine SP-B). Also studied in the same rat model and found to have lower activity than either S-MB/MB synthetic surfactants or Infasurf® were the clinical surfactant Survanta® and UCLA KL4 (synthetic lipids plus 3% KL4 peptide modeled after clinical Surfaxin®) (data not shown). Similar recent studies in ventilated, lavaged and surfactant-deficient rabbits have demonstrated that the in vivo surface activity of synthetic lung surfactant formulated with S-MB alone or with a SP-C mimic is at least equivalent or superior to its native components [96].

New SP-B Peptide Design Strategies

Future SP-B peptide design based on the saposin fold might include the incorporation of nonnative amino acids in the MB and S-MB peptides. For example, the substitution of very hydrophobic, nonnative amino acid residues for the native hydrophobic amino acids may produce helix-hairpin-hairpin constructs with a more defined interaction towards different classes of surfactant lipids. In turn, this might enhance the in vitro and in vivo activities of the lipid-peptide mimic dispersions. The helix-hairpin-helix conformation of both the MB and S-MB sequences also affords the possibility of bio-conjugate chemical modification such as polyethylene glycol covalent attachment and chemically linked lipids. Such covalent attachments to the peptide scaffold may make the peptides more resistant to classical surfactant inhibitors, including albumin [96]. The recent finding that native SP-B forms higher-ordered ring structures composed of 5 or 6 covalent dimers that may profoundly influence surface properties [97] should certainly be considered in future design strategies.

Conclusions

The SAPLIP family of proteins share an overall 3D folding pattern based on secondary structures and disulfide connectivity information. Using the saposin design, we have developed synthetic, disulfide cross-linked peptide constructs (e.g., the 34-residue "Mini-B" or "MB" and the 41-residue "Super Mini-B" or "S-MB"), which not only mimic the structure of the SP-B leaf containing the N- and C-terminal regions, but also demonstrate high surfactant activities in in vitro and in vivo assays. SP-B activity is vitally important in lung surfactant and respiratory function. Highly functional "short-cut" versions of full-length SP-B (e.g., MB and S-MB) offer the opportunity to formulate synthetic lung surfactant preparations to reverse surfactant deficiency and/or dysfunction in neonatal RDS and ALI/ARDS.

Acknowledgments

This work was supported by the National Institutes of Health (grants R02HL055534, R01HL092158, and R01ES015330).

Disclosure Statement

The authors declare no conflicts of interest.

References

1 Notter RH: Lung Surfactants: Basic Science and Clinical Applications. New York, Marcel Dekker, 2000.
2 Whitsett JA, Weaver TJ: Mechanisms of disease: hydrophobic surfactant proteins in lung function and disease. N Engl J Med 2002;347:2141–2148.
3 Munford RS, Sheppard PO, O'Hara PJ: Saposin-like proteins (SAPLIP) carry out diverse functions on a common backbone structure. J Lipid Res 1995;36:1653–1663.
4 Liepinsh E, Andersson M, Ruysschaert JM, Otting G: Saposin fold revealed by the NMR structure of NK-lysin. Nat Struct Biol 1997;4:793–795.
5 de Alba E, Weiler S, Tjandra N: Solution structure of human saposin C: pH-dependent interaction with phospholipid vesicles. Biochemistry 2003;42:14729–14740.
6 Hawkins CA, de Alba E, Tjandra N: Solution structure of human saposin C in a detergent environment. J Mol Biol 2005;346:1381–1392.

7 Ahn VE, Faull KF, Whitelegge JP, Fluharty AL, Prive GG: Crystal structure of saposin B reveals a dimeric shell for lipid binding. Proc Natl Acad Sci USA 2003;100:38–43.
8 Ahn VE, Leyko P, Alattia JR, Chen L, Prive GG: Crystal structures of saposins A and C. Protein Sci 2006;15:1849–1857.
9 Anderson DH, Sawaya MR, Cascio D, Ernst W, Modlin R, Krensky A, Eisenberg D: Granulysin crystal structure and a structure-derived lytic mechanism. J Mol Biol 2003;325:355–365.
10 Hecht O, Van Nuland N, Schleinkofer K, Dingley AJ, Bruhn H, Leippe M, Grotzinger J: Solution structure of the pore-forming protein of entamoeba histolytica. J Biol Chem 2004;279:17834–17841.
11 Bruhn H: A short guided tour through functional and structural features of saposin-like proteins. Biochem J 2005;389:249–257.
12 Zaltash S, Palmblad M, Curstedt T, Johansson J, Persson B: Pulmonary surfactant protein B: a structural model and a functional analogue. Biochim Biophys Acta 2000;1466:179–186.
13 Walther FJ, Gordon LM, Zasadzinski JA, Sherman MA, Waring AJ: Surfactant protein B and C analogues. Mol Genet Metab 2000;71:342–351.
14 Waring AJ, Walther FJ, Gordon LM, Hernandez-Juviel JM, Hong T, Sherman MA, Alonso C, Alig T, Braun A, Bacon D, Zasadzinski JA: The role of charged amphipathic helices in the structure and function of surfactant protein B (SP-B). J Peptide Res 2005;66:364–374.
15 Zhang Y, Skolnick J: TM-align: a protein structure alignment algorithm based on TM-score. Nucleic Acids Res 2005;33:2302–2309.
16 Yang J, Yan R, Roy A, Xu D, Poisson J, Zhang Y: The I-TASSER Suite: protein structure and function prediction. Nat Methods 2015;12:7–8.
17 Gordon LM, Horvath S, Longo ML, Zasadzinski JA, Taeusch W, Faull K, Leung C, Waring AJ: Conformation and molecular topography of the N-terminal segment of surfactant protein B in structure-promoting environments. Protein Sci 1996;5:1662–1675.
18 Gordon LM, Lee KYC, Lipp MM, Zasadzinski JA, Walther FJ, Sherman MA, Waring AJ: Conformational mapping of the N-terminal segment of surfactant protein B in lipid using ^{13}C-enhanced Fourier transform infrared spectroscopy. J Peptide Res 2000;55:330–347.
19 Walther FJ, Waring AJ, Hernandez-Juviel JM, Gordon LM, Wang Z, Jung CL, Ruchala P, Clark AP, Smith WM, Sharma S, Notter RH: Critical structural and functional roles for the N-terminal insertion sequence in surfactant protein B analogs. PLoS One 2010;5:e8672.
20 Kurutz JW, Lee KY: NMR structure of lung surfactant peptide SP-B(11–25). Biochemistry 2002;41:9627–9636.
21 Sarker M, Waring AJ, Walther FJ, Keough KMW, Booth V: Structure of Mini-B, a functional fragment of surfactant protein B, in detergent micelles. Biochemistry 2007;46:11047–11056.
22 Bertani P, Vidovic V, Yang TC, Rendell J, Gordon LM, Waring AJ, Bechinger B, Booth V: Orientation and depth of surfactant protein B C-terminal helix in lung surfactant bilayers. Biochim Biophys Acta 2012;1818:1165–1172.
23 Walther FJ, Waring AJ, Sherman MA, Zasadzinski JA, Gordon LM: Hydrophobic surfactant proteins and their analogues. Neonatology 2007;91:303–310.
24 Walther FJ, Waring AJ, Hernandez-Juviel J, Gordon LM, Schwan AL, Jung C-L, Chang Y, Wang Z, Notter RH: Dynamic surface activity of a fully synthetic phospholipase-resistant lipid/peptide lung surfactant. PLoS One 2007;2:e1039.
25 Notter RH, Finkelstein JN, Holm BA: Lung Injury: Mechanisms, Pathophysiology and Therapy. Boca Raton, Taylor Francis Group, 2005.
26 Bernard GR, Artigas A, Brigham KL, Carlet J, Falke K, Hudson L, Lamy M, Legall JR, Morris A, Spragg R: The American-European Consensus Conference on ARDS: definitions, mechanisms, relevant outcomes, and clinical trial coordination. Am J Respir Crit Care Med 1994;149:818–824.
27 Ware LB, Matthay MA: The acute respiratory distress syndrome. N Engl J Med 2000;342:1334–1348.
28 Rubenfeld GD, Caldwell E, Peabody E, Weaver J, Martin DP, Neff M, Stern EJ, Hudson LJ: Incidence and outcomes of acute lung injury. N Engl J Med 2005;353:1685–1693.
29 Goss CH, Brower RG, Hudson LD, Rubenfeld GD; ARDS Network: Incidence of acute lung injury in the United States. Crit Care Med 2003;31:1607–1611.
30 Flori HR, Glidden DV, Rutherford GW, Matthay MA: Pediatric acute lung injury. Prospective evaluation of risk factors associated with mortality. Am J Respir Crit Care Med 2005;171:995–1001.
31 Polin RA, Carlo WA; Committee on Fetus and Newborn; American Academy of Pediatrics: Surfactant replacement therapy for preterm and term neonates with respiratory distress. Pediatrics 2014;133:156–163.
32 Willson DF, Chess PR, Notter RH: Surfactant for pediatric acute lung injury. Pediatr Clin North Am 2008;55:545–575.
33 Anzueto A, Baughman RP, Guntupalli KK, Weg JG, Wiedemann HP, Raventos AA, Lemaire F, Long W, Zaccardelli DS, Pattishall EN; Exosurf ARDS Sepsis Study Group: Aerosolized surfactant in adults with sepsis-induced acute respiratory distress syndrome. N Engl J Med 1996;334:1417–1421.
34 Gregory TJ, Steinberg KP, Spragg R, Gadek JE, Hyers TM, Longmore WJ, Moxley MA, Cai GZ, Hite RD, Smith RM, Hudson LD, Crim C, Newton P, Mitchell BR, Gold AJ: Bovine surfactant therapy for patients with acute respiratory distress syndrome. Am J Respir Crit Care Med 1997;155:109–131.
35 Willson DF, Thomas NJ, Markovitz BP, DiCarlo JV, Pon S, Jacobs BR, Jefferson LS, Conaway MR, Egan EA: Effect of exogenous surfactant (calfactant) in pediatric acute lung injury: a randomized controlled trial. JAMA 2005;293:470–476.

36 Spragg RG, Lewis JF, Wurst W, Hafner D, Baughman RP, Wewers MD, Marsh JJ: Treatment of acute respiratory distress syndrome with recombinant surfactant protein C surfactant. Am J Respir Crit Care Med 2003;167:1562–1566.
37 Notter RH, Schwan AL, Wang Z, Waring AJ: Novel phospholipase-resistant lipid/peptide synthetic lung surfactants. Mini Rev Med Chem 2007;7:932–944.
38 Schwan AL, Singh SP, Davy JA, Waring AJ, Gordon LM, Walther FJ, Wang Z, Notter RH: Synthesis and activity of a novel diether phosphonoglycerol in phospholipase-resistant synthetic lipid:peptide lung surfactants. Med Chem Commun 2011;2:1167–1173.
39 Kim DK, Fukuda T, Thompson BT, Cockrill B, Hales C, Bonventre JV: Bronchoalveolar lavage fluid phospholipase A_2 activities are increased in human adult respiratory distress syndrome. Am J Physiol 1995;269:L109–L118.
40 Holm BA, Kelcher L, Liu M, Sokolowski J, Enhorning G: Inhibition of pulmonary surfactant by phospholipases. J Appl Physiol 1991;71:317–321.
41 Touqui L, Arbibe L: A role for phospholipase A_2 in ARDS pathogenesis. Mol Med Today 1999;5:244–249.
42 Sato A, Ikegami M: SP-B and SP-C containing new synthetic surfactant for treatment of extremely immature lamb lung. PLoS One 2012;7:e39392.
43 Seehase M, Collins JJ, Kuypers E, Jellema RK, Ophelders DR, Ospina OL, Perez-Gil J, Bianco F, Garzia R, Razzetti R, Kramer BW: New surfactant with SP-B and C analogs gives survival benefit after inactivation in preterm lambs. PLoS One 2012;7:e47631.
44 Romero EJ, Moya FR, Tuvim MJ, Alcorn JL: Interaction of an artificial surfactant in human pulmonary epithelial cells. Pediatr Pulmonol 2005;39:167–177.
45 Poelma DL, Walther FJ, Waring AJ, Haitsma JJ, Zimmermann LJ, Lachmann B, van Iwaarden JF: Effect of SP-B peptides on the uptake of liposomes by alveolar cells. Neonatology 2007;91:233–240.
46 Wang Z, Chang Y, Schwan AL, Notter RH: Activity and inhibition resistance of a phospholipase-resistant synthetic exogenous surfactant in excised rat lungs. Am J Respir Cell Mol Biol 2007;37:387–394.
47 Oosterlaken-Dijksterhuis MA, van Eijk M, van Golde LMG, Haagsman HP: Lipid mixing is mediated by the hydrophobic surfactant protein SP-B but not by SP-C. Biochim Biophys Acta 1992;1110:45–50.
48 Walther FJ, Hernandez-Juviel J, Bruni R, Waring A: Spiking Survanta with synthetic surfactant peptides improves oxygenation in surfactant-deficient rats. Am J Respir Crit Care Med 1997;156:855–861.
49 Clark JC, Weaver TE, Iwamoto HS, Ikegami M, Jobe AH, Hull WM, Whitsett JA: Decreased lung compliance and air trapping in heterozygous SP-B-deficient mice. Am J Respir Cell Mol Biol 1997;16:46–52.
50 Hamvas A, Cole FS, deMello DE, Moxley M, Whitsett JA, Colten HR, Nogee LM: Surfactant protein B deficiency: antenatal diagnosis and prospective treatment with surfactant replacement. J Pediatr 1994;125:356–361.
51 Hamvas A, Nogee LM, Mallory GB Jr, Spray TL, Huddleston CB, August A, Dehner LP, deMello DE, Moxley M, Nelson R, Cole FS, Colten HR: Lung transplantation for treatment of infants with surfactant protein B deficiency. J Pediatr 1997;130:231–239.
52 Ikegami M, Whitsett JA, Martis PC, Weaver TE: Reversibility of lung inflammation caused by SP-B deficiency. Am J Physiol Lung Cell Mol Physiol 2005;289:L962–L970.
53 Andersson M, Curstedt T, Jornvall H, Johansson J: An amphipathic helical motif common to tumourolytic polypeptide NK-lysin and pulmonary surfactant polypeptide SP-B. FEBS Lett 1995;362:328–332.
54 Vandenbussche G, Clercx A, Clercx M, Curstedt T, Johansson J, Jornvall H, Ruysschaert J-M: Secondary structure and orientation of the surfactant protein SP-B in a lipid environment: a Fourier transform infrared spectroscopy study. Biochemistry 1992;31:9169–9176.
55 Lipp MM, Lee KYC, Zasadzinski JA, Waring AJ: Phase and morphology changes in lipid monolayers induced by SP-B protein and its amino-terminal peptide. Science 1996;273:1196–1199.
56 Longo ML, Bisagno AM, Zasadzinski JA, Bruni R, Waring AJ: A function of lung surfactant protein SP-B. Science 1993;261:453–456.
57 Lipp MM, Lee KYC, Takamoto DY, Zasadzinski JAN, Waring AJ: Coexistence of buckled and flat monolayers. Physical Rev Lett 1998;81:1650–1653.
58 Frey SL, Pocivavsek L, Waring AJ, Walther FJ, Hernandez-Juviel JM, Ruchala P, Lee KY: Functional importance of the NH2-terminal insertion sequence of lung surfactant protein B. Am J Physiol Lung Cell Mol Physiol 2010;298:L335–L347.
59 Waring AJ, Taeusch HW, Bruni R, Amirkhanian JD, Fan BR, Stevens R, Young J: Synthetic amphipathic sequences of surfactant protein-B mimic several physicochemical and in vivo properties of native pulmonary surfactant proteins. Peptide Res 1989;2:308–313.
60 Gupta M, Hernandez-Juviel JM, Waring AJ, Bruni R, Walther FJ: Comparison of functional efficacy of surfactant protein B analogues in lavaged rats. Eur Respir J 2000;16:1129–1133.
61 Gupta M, Hernandez-Juviel JM, Waring AJ, Walther FJ: Function and inhibition sensitivity of the N-terminal segment of surfactant protein B (SP-B1-25) in preterm rabbits. Thorax 2001;56:871–876.
62 Walther FJ, Hernandez-Juviel JM, Gordon LM, Sherman MA, Waring AJ: Dimeric surfactant protein B peptide sp-b(1-25) in neonatal and acute respiratory distress syndrome. Exp Lung Res 2002;28:623–640.
63 Ryan MA, Qi X, Serrano AG, Ikegami M, Perez-Gil J, Johansson J, Weaver TE: Mapping and analysis of the lytic and fusogenic domains of surfactant protein B. Biochemistry 2005;44:861–872.
64 Bruni R, Taeusch HW, Waring AJ: Surfactant protein B: lipid interactions of synthetic peptides representing the amino-terminal amphipathic domains. Proc Natl Acad Sci USA 1991;88:7451–7455.

65 Gustafsson M, Vandenbussche G, Curstedt T, Ruysschaert JM, Johansson J: The 21-residue surfactant peptide (LysLeu4)4Lys(KL4) is a transmembrane alpha-helix with a mixed nonpolar/polar surface. FEBS Lett 1996; 384:185–188.
66 Kang JH, Lee MK, Kim KL, Hahm K-S: The relationship between biophysical activity and the secondary structure of synthetic peptides from the pulmonary surfactant protein SP-B. Biochem Mol Biol Int 1996;40:617–627.
67 Booth V, Waring AJ, Walther FJ, Keough KMW: NMR structures of the C-terminal segment of surfactant protein B in detergent micelles and hexafluoro-2-propanol. Biochemistry 2004;43:15187–15194.
68 Revak SD, Merritt TA, Hallman M, Heldt G, La Polla RJ, Hoey K, Houghten RA, Cochrane CG: The use of synthetic peptides in the formation of biophysically and biologically active pulmonary surfactants. Pediatr Res 1991;29: 460–465.
69 Baatz JE, Sarin V, Absolom DR, Baxter C, Whitsett JA: Effects of surfactant-associated protein SP-B synthetic analogs on the structure and surface activity of model membrane bilayers. Chem Phys Lipids 1991;60:163–178.
70 Cochrane CG, Revak SD: Pulmonary surfactant B (SP-B): Structure-function relationships. Science 1991;254: 566–568.
71 Cochrane CG, Revak SD, Merritt TA, Heldt GP, Hallman M, Cunningham MD, Easa D, Pramanik A, Edwards DK, Alberts MS: The efficacy and safety of KL4-surfactant in preterm infants with respiratory distress syndrome. Am J Respir Crit Care Med 1996;153:404–410.
72 Moya FR, Gadzinowski J, Bancalari E, Salinas V, Kopelman B, Bancalari A, Kornacka MK, Merritt TA, Segal R, Schaber CJ, Tsai H, Massaro J, d'Agostino R; International Surfaxin Collaborative Study Group: A multicenter, randomized, masked, comparison trial of lucinactant, colfosceril palmitate, and beractant for the prevention of respiratory distress syndrome among very preterm infants. Pediatrics 2005;115:1018–1029.
73 Sinha SK, Lacaze-Masmonteil T, Soler A, Wiswell TE, Gadzinowski J, Hajdu J, Bernstein G, Sanchez-Luna M, Segal R, Schaber CJ, Massaro J, d'Agostino R: A multicenter, randomized, controlled trial of lucinactant versus poractant alfa among very premature infants at high risk for respiratory distress syndrome. Pediatrics 2005; 115:1030–1038.
74 Cai P, Flach CR, Mendelsohn R: An infrared reflection-absorption spectroscopy study of the secondary structure in (KL4)4K, a therapeutic agent for respiratory distress syndrome, in aqueous monolayers with phospholipids. Biochemistry 2003;42:9446–9452.
75 Saenz A, Canadas O, Bagatolli LA, Johnson ME, Casals C: Physical properties and surface activity of surfactant-like membranes containing the cationic and hydrophobic peptide KL4. FEBS J 2006;273:2515–2527.
76 Marcelino AM, Gierasch LM: Roles of beta-turns in protein folding: from peptide models to protein engineering. Biopolymers 2008;89:380–391.
77 Kountouris P, Hirst JD: Prediction of backbone dihedral angles and protein secondary structure using support vector machines. BMC Bioinformatics 2009;10:437.
78 Kountouris P, Hirst JD: Predicting beta-turns and their types using predicted backbone dihedral angles and secondary structures. BMC Bioinformatics 2010;11:407.
79 Biswas N, Waring AJ, Walther FJ, Dluhy RA: Structure and conformation of the disulfide bond in dimeric lung surfactant peptides SP-B_{1-25} and SP-B_{8-25}. Biochim Biophys Acta 2007;1768:1070–1082.
80 Serrano AG, Ryan M, Weaver TE, Perez-Gil J: Critical structure-function determinants within the N-terminal region of pulmonary surfactant protein SP-B. Biophys J 2006;90:238–249.
81 Fields CG, Lloyd DH, McDonald RL, Ottenson KM, Nobel RL: HBTU activation for automated Fmoc solid-phase peptide synthesis. Peptide Res 1991;4:95–101.
82 Carpino LA, Chao H-G, Chassemi S, Mansour EME, Riemer C,Warrass R, Sadat-Aalaee D, Truran GA, Imazumi H, Wenshuch H, Beyermann M, Bienert M, Shroff H, Albericio F, Triolo SA, Sole NA, Kates SA: Novel carboxylic acid and carboxamide protective groups based on the exceptional stabilization of the cyclopropylmethyl cation. J Org Chem 1995;60:7718–7719.
83 Waring A, Faull L, Leung C, Chang-Chien A, Mercado P, Taeusch HW, Gordon L: Synthesis, secondary structure and folding of the bend region of lung surfactant protein B. Peptide Res 1996;9:28–31.
84 Holten-Andersen N, Michael HJ, Walther FJ, Waring AJ, Ruchala P, Notter RH, Lee KY: KL_4 peptide induces reversible collapse structures on multiple length scales in model lung surfactant. Biophys J 2011;101:2957–2965.
85 Vandenbussche G, Clercx A, Curstedt T, Johansson J, Jornvall H, Ruysschaert JM: Structure and orientation of the surfactant-associated protein C in a lipid bilayer. Eur J Biochem 1992;203:201–209.
86 Johansson J, Szyperski T, Curstedt T, Wuthrich K: The NMR structure of the pulmonary surfactant-associated polypeptide SP-C in an apolar solvent contains a valyl-rich alpha-helix. Biochemistry 1994;33:6015–6023.
87 Johansson J: Structure and properties of surfactant protein C. Biochim Biophys Acta 1998;1408:161–172.
88 Trovato A, Seno F, Tosatto SCE: The PASTA server for protein aggregation prediction. Protein Eng Des Sel 2007;20:521–523.
89 Trovato A, Chiti F, Maritan A, Seno F: Insight into the structure of amyloid fibrils from the analysis of globular proteins. PLoS Comput Biol 2006;2:e170.
90 Chen R, Li L, Weng Z: ZDOCK: An initial-stage protein-docking algorithm. Proteins 2003;52:80–87.
91 Lyskov S, Gray JJ: The RosettaDock server for local protein-protein docking. Nucleic Acids Res 2008;36:W233–W238.

▶92 Schurch S, Bachofen H, Goerke J, Possmayer F: A captive bubble method reproduces the in situ behavior of lung surfactant monolayers. J Appl Physiol 1989;67:2389–2396.
▶93 Schurch S, Bachofen H, Goerke J, Green F: Surface properties of rat pulmonary surfactant studied with the captive bubble method: adsorption, hysteresis, stability. Biochim Biophys Acta 1992;1103:127–136.
▶94 Walther FJ, Hernandez-Juviel JM, Gordon LM, Waring AJ, Stenger P, Zasadzinski JA: Comparision of three lipid formulations for synthetic surfactant with a surfactant protein B analog. Exp Lung Res 2005;31:563–579.
▶95 Soll RF: Surfactant therapy in the USA: trials and current routines. Biol Neonate 1997;71:1–7.
▶96 Notter RH, Wang Z, Walther FJ: Activity and biophysical inhibition resistance of a novel synthetic lung surfactant containing Super-Mini-B DATK peptide. PeerJ 2016;4:e1528.
▶97 Olmeda B, García-Álvarez B, Gómez MJ, Martínez-Calle M, Cruz A, Pérez-Gil J: A model for the structure and mechanism of action of pulmonary surfactant protein B. FASEB J 2015;29:4236–4247.